Physiologia Plantarum

ORIGINAL RESEARCH OPEN ACCESS

A Mitochondrially Related Plastidial Transporter Regulates Photosynthesis in the Diatom *Phaeodactylum tricornutum*

Cécile Giustini[1] | Davide Dal Bo[1] | Mattia Storti[1] | Mick Van Vlierberghe[2] | Denis Baurain[2] | Pierre Cardol[3] | Youjun Zhang[4] | Alisdair R. Fernie[4] | Duncan Fitzpatrick[5] | Eva-Mari Aro[5] | Guillaume Allorent[1] | Pascal Albanese[1] | Dimitri Tolleter[1] | Gilles Curien[1] | Giovanni Finazzi[1]

[1]University Grenoble Alpes, CNRS, INRAE, CEA, IRIG-LPCV, Grenoble, France | [2]InBioS-PhytoSYSTEMS, Eukaryotic Phylogenomics, University of Liège, Liège, Belgium | [3]InBioS-PhytoSYSTEMS, Génétique et Physiologie Des Microalgues, University of Liège, Liège, Belgium | [4]Max-Planck-Institut Für Molekulare Pflanzenphysiologie, Potsdam Science Park, Potsdam-Golm, Germany | [5]Department of Life Technologies, Molecular Plant Biology, University of Turku, Turku, Finland

Correspondence: Dimitri Tolleter (dimitri.tolleter@cea.fr) | Giovanni Finazzi (giovanni.finazzi@cea.fr)

Received: 30 July 2025 | **Revised:** 22 October 2025 | **Accepted:** 26 October 2025

Handling Editor: A. Krieger-Liszkay

Funding: This work was supported by European Union's Horizon 2020 Research and Innovation Program (101066400; PHOTO-LINK), Plankton Project (101099192), European Research Council (833184; Chloro-Mito), CNRS Momentum Program and Jane and Aatos Erkko Foundation.

Keywords: diatoms | MCF transporter | photosynthesis regulation | plastid–mitochondria interaction

ABSTRACT

Eukaryotic phototrophs depend on the activity of two engines (the plastid and the mitochondrion) to generate the energy required for cellular metabolism. Because of their overlapping functions, both activities must be closely coordinated. At the plastid level, optimisation occurs through alternative electron transport, the diversion of excess electrons from the linear transport chain and metabolic exchanges. A similar process takes place in the mitochondria, with documented evidence of energy and redox equivalents being exchanged between the two organelles. Organelle-organelle energy interactions at the physiological level are well established in diatoms, an ecologically significant member of phytoplankton. Yet the molecular components involved in this process remain largely unknown. Here, we identify a mitochondrial carrier family (MCF) transporter, MCFc, located at the plastid envelope of *Phaeodactylum tricornutum*, which seems to be widely distributed in complex algae. We then compare the performance of a wild-type and a mutant lacking MCFc. An analysis of spectroscopic and oxygen exchange data unveiled altered energetic interactions in the mutant, suggesting that MCFc plays a role in plastid-mitochondrion communication. In silico analysis of MCFc implies a similar substrate-specific model to that of ADP/ATP carriers, although distinct motif differences in MCFc indicate potential variations in its function, with possible substrates including arginine, aspartate/glutamate or citrate/isocitrate. Together, these findings support a role for mitochondrial energy metabolism in sustaining diatom photosynthesis, likely mediated by MCFc, though further investigation is needed to determine the precise mechanism.

1 | Introduction

Photosynthesis relies on light-driven electron flow to generate bioavailable reducing power (NADPH), which is subsequently utilised by the Calvin–Benson–Bassham (CBB) cycle. Photosynthesis also requires ATP, but the ATP/NADPH ratio generated by linear electron flow is thought to be insufficient to fuel CO_2 assimilation (reviewed in Alric 2010 and

Petersen et al. 2012). This ratio is changeable via the modulation of linear (LEF) and alternative electron flow, comprising cyclic electron flow (CEF) around PSI (Shikanai 2007) and the 'water–water cycles' (i.e., flavodiiron proteins and Mehler reaction). Exchange mechanisms between plastids and mitochondria have been characterised in land plants (Hoefnagel et al. 1998a, 1998b). Thanks to these mechanisms, the ATP/NADPH ratio undergoes continuous adjustments according to light availability and cellular metabolic demands. As observed in some microalgae, the close special association between plastids and mitochondria in diatoms has led to the hypothesis that exchanges between the two organelles occur through direct physical contacts, as shown by electron microscopy (EM) and focused ion beam milling (FIB)-EM imaging (Bailleul et al. 2015). However, recent results obtained from samples prepared in more native conditions (cryo FIB-SEM) suggest that this may not be the case (Uwizeye et al. 2021), reopening the question of plastid-mitochondria interactions. In this context, we decided to re-evaluate the metabolic interaction mechanisms between the two organelles in diatoms, aiming at identifying specific molecular transporters. By combining molecular, bioinformatic and physiological analyses, we identified a candidate transporter (mitochondrial carrier family chloroplastic, MCFc) and characterised the phenotypic features of mutant lines lacking this function in the diatom *Phaeodactylum tricornutum*.

The mitochondrial carrier family (MCF) proteins are a group of nuclear-encoded and membrane-embedded proteins usually localised at the inner membrane of mitochondria. These proteins, small carriers with a molecular mass of about 30–34 kDa, facilitate the selective transport of essential metabolites, such as di- and tricarboxylates, keto acids, amino acids, nucleotides and coenzymes/cofactors, across the inner mitochondrial membrane, thereby linking mitochondria and the cytosol (Palmieri et al. 2011; Palmieri 2013). This connection is vital, as many physiological processes require the cooperation of both intra- and extra-mitochondrial pathways.

All MCF proteins share common structural features, consisting of three tandemly repeated homologous domains, each about 100 amino acids in length. Each domain contains two hydrophobic stretches separated by hydrophilic regions, with the signature sequence motif PX[D/E]XX[K/R]X[K/R] (PROSITE PS50920, PFAM PF00153, IPR00193), which is used to recognise MCF members (Satre et al. 2007). Many MCFs catalyse 1:1 exchange reactions (antiport), though other transport modes are also possible, like uniport and H^+-compensated anion symport (Palmieri and Pierri 2010). MCF transporters are broadly classified as either electrophoretic (electrogenic) or electroneutral, depending on the nature of the solute exchange they mediate. For instance, ADP/ATP and aspartate/glutamate carriers are electrogenic, whereas carriers for inorganic phosphate (Pi), glutamate, GTP/GDP, oxoglutarate and ornithine function in an electroneutral manner. Given their role in transporting a wide range of solutes and linking multiple metabolic pathways across cellular compartments, it is plausible that our candidate MCF transporter belongs to this family, or at least shares key functional characteristics with its members.

2 | Materials and Methods

2.1 | *P. tricornutum* Cultivation

P. tricornutum (Pt1, CCAP 1055/3) cells were cultivated following the protocol outlined in Villanova et al. 2021. They were grown in a modified enriched Seawater Artificial Water (ESAW) containing a concentration of N and P 10 times higher compared to the regular ESAW medium (Harrison et al. 1980) modified in Berges et al. (2001), added Cu to 3.92×10^{-8} M and removed silicate. Cells were maintained at 19°C under a light intensity of 40 µmol photon $m^{-2} s^{-1}$ with a 12 h light/12 h dark photoperiod and shaking at 90 rpm. They were collected in the exponential phase and concentrated to a density of $2–5 \times 10^6$ cells per mL.

2.2 | Phylogenetic Analysis

Candidate proteins were identified using ASAFind (Gruber et al. 2015), a bioinformatic tool designed to detect nuclear-encoded plastid-targeted proteins in complex algae. ASAFind integrates results from SignalP (Petersen et al. 2011) to detect N-terminal signal peptides and recognises conserved ASAFAP-like motifs required for ER-mediated plastid import in diatoms. We screened for transporters with predicted plastid targeting and functional homology to ATP or redox transporters, narrowing our focus to MCF homologs.

The broadly sampled orthogroup OG0001460 (including *P. tricornutum* MCFc) obtained in Van Vlierberghe, Philippe, and Baurain (2021) was aligned with MAFFT (Katoh and Standley 2013) and its largest photosynthetic subtree (=clan OG0001460-8) was enriched using Forty-Two (Irisarri et al. 2017; Simion et al. 2017) with sequences from 172 high-quality transcriptomes of plastid-bearing lineages resulting from the decontamination, pooling and dereplication of the 678 MMETSP samples (Keeling et al. 2014) performed in Van Vlierberghe, Di Franco, et al. (2021). Amino-acid alignments were filtered with ali2phylip.pl. from the Bio::MUST::Core software package available on CPAN (https://metacpan.org/dist/Bio-MUST-Core) and used to infer phylogenetic trees using IQ-TREE 2 (Minh et al. 2020) with the ultrafast bootstrap option under the C20 (Le et al. 2008) (or LG4X Le et al. 2012) model. Raw trees, including progressively less outgroup sequences, were then automatically rooted, annotated, colourised and collapsed based on NCBI Taxonomy using format-tree.pl. (also from Bio::MUST::Core) and uploaded to ITOL for further annotation and graphical rendering (Letunic and Bork 2024). Alignments and trees are available at Figshare under DOI: https://doi.org/10.6084/m9.figshare.28207955.

2.3 | Localisation

The construction of the MCFc::GFP fusion was performed as in Liu et al. (2025). To visualise mitochondria, the mitochondrial probe TMRM (tetramethylrhodamine, methyl ester, perchlorate, Invitrogen MitoProbe) was added at a concentration of 100 nM. Imaging was performed using a Zeiss LSM 900 confocal microscope equipped with ZEN software (version 3.0,

Blue edition). A 63×/1.4 M27 objective lens was used in confocal mode with an Airyscan 2 detector to ensure fast acquisition without compromising sensitivity, aided by a collimation optic. Excitation for chlorophyll fluorescence was provided by a 405 nm blue laser, and emission was collected between 650 and 700 nm. GFP visualisation involved 488 nm excitation with fluorescence collected between 500 and 536 nm, while for TMRM, excitation was at 561 nm with fluorescence collected between 570 and 613 nm. Images shown correspond to maximum intensity projections from Z-stacks, allowing clear visualisation of fluorescence signal distribution across the chloroplast volume.

The protocol for ultrastructural expansion microscopy (U-ExM) has been modified from Klena et al. (2023). *P. tricornutum* cultures were grown to a concentration of 6.0×10^6 cells/200 µL, and then allowed to sediment to a 12 mm round Poly-D-Lysine (A3890401, Gibco) coated coverslip for 5 min. Thereafter, the following steps were performed:

1. Protein anchoring: Coverslips were incubated for 3 h and 30 min in 1.4% FA/2% acrylamide (AA) at 37°C in a 12-well plate.
2. Gelation: Performed in monomer solution (21% sodium acrylate (wt/wt); 10% acrylamide (A4058, SIGMA); 0.1% N′-methylene-bis-acrylamide (M1533, SIGMA) in PBS) for 1 h at 37°C.
3. Denaturation: Gel was transferred to the denaturation buffer for 15 min at RT and then shifted to 95°C for 1 h.
4. First gel expansion and antibody labelling: After denaturation, gels were incubated in ddH_2O at room temperature for 30 min (twice), then left in ddH_2O overnight for complete expansion. The next day, gels were washed in PBS twice for 15 min to remove excess water. Three different primary antibodies were used: anti-GFP at 1/200 dilution (Invitrogen A11122, host: rabbit), anti-PsbA (thylakoid, PSII) at 1/500 dilution (Agrisera: AAS01016, host: hen) and anti-RbcL (pyrenoid, Rubisco sub-unit) at 1/500 dilution (Agrisera: AS01017, host: hen). The primary antibody incubation was performed in PBS-0.1% tween20 at 4°C overnight, followed by four 10-min washes in PBS-Tween 0.1%. Incubation with the secondary antibody coupled with fluorochrome, goat anti-rabbit IgG (H + L) highly cross-adsorbed secondary antibody, Alexa Fluor Plus 647 (A32733, Thermo fisher) or goat anti-chicken IgY (H + L) cross-adsorbed secondary antibody, Alexa Fluor Plus 488 (A32931, Thermo fisher), was performed for 2 h and 30 min at RT, followed by four additional 10-min washes in PBS-0.1%. Tween20 (all wash steps were performed with 100 rpm shaking at 20°C).
5. NHS-ester staining: Directly after antibody staining, gels were incubated in 565 NHS-ester solution (Merck: 72464) at 20 µg mL^{-1} in PBS for 2 h and 30 min at room temperature on a shaker. The gels were then washed four times for 10 min with PBS-Tween 0.1% and the gels were incubated in ddH_2O at room temperature for 30 min, then left in ddH_2O. A third round of expansion was performed in water before imaging.
6. Sample mounting and imaging: 1 × 1 cm gel pieces were cut from the expanded gel and attached to 24 mm round poly-D-lysine-coated coverslips to prevent gel sliding and avoid drift during imaging. Imaging was done on a Zeiss LSM 900 microscope. Image has been processed with the ZEN software (version 3.0, Blue edition)

2.4 | Construction of the MCFc Mutants

P. tricornutum mutant MCFc strains have been generated through CRISPR/Cas9 according to the protocol described in Giustini et al. (2024).

The following target sequence was designed using the PhytoCRISP-Ex web tool (Rastogi et al. 2016): 5′-GTCAGCCGAGAAGCCGACGA-3′. The target sequences were inserted into the pKSdiaCas9_sgRNA plasmid (Addgene #74923). The resulting plasmids and the pAF6 plasmid, conferring a resistance to zeocin (100 µg mL^{-1}) were coated on tungsten beads and used for biolistic transformation of the cells with the PDS-100/He system (Bio-Rad; 1,672,257). Genomic DNA from zeocin-resistant transformants was extracted, amplified by PCR using the following primers 5′-ACGCGCATGTAGTTACAGTTAGCGTATTT-3′ (forward) and 5′-CCTGGGTAGCGGGAAGCGTTT-3′ (reverse) and sequenced for mutant identification.

2.5 | Protein Extraction and Immunoblot Analysis

Proteins were extracted and analysed as described in Seydoux et al. (2022). In short, cells (approximately 8.0×10^6) were pelleted and resuspended in 50 mM HEPES buffer (pH 7.5) supplemented with an EDTA-free protease inhibitor cocktail (cOmplete, Roche). Cell lysis was achieved using a Precellys Evolution Homogeniser (Bertin) with the following settings: 2 cycles of 30 s at *x*, with a 30-s pause between cycles at 4°C. Proteins were then precipitated using 80% acetone by centrifugation at 4°C and resuspended in lysis buffer (100 mM Tris–HCl, pH 6.8, 4% SDS, 20 mM EDTA) supplemented with the protease inhibitor.

For immunoblot analysis, 10–30 µg of protein were separated by SDS-PAGE in Tris-Glycine buffer (25 mM Tris, 190 mM glycine, 0.05% SDS). Proteins were transferred onto a nitrocellulose membrane using the same buffer supplemented with 20% ethanol for 80 min at 100 V. Immunodetection was performed using a guinea pig anti-MCFc serum raised against the full-length recombinant protein (dilution 1:3000; Charles River Laboratories, Strasbourg, France) and an anti-AtpB antibody (dilution 1:5000; AS05085; Agrisera). Detection was carried out with an HRP-conjugated secondary antibody, and the signal was developed using the Clarity Western ECL Substrates kit. Images of the blots were captured using a CCD imager (ChemiDoc MP Imaging System, Bio-Rad).

2.6 | Oxygen Exchange Measurements

Oxygen consumption (respiration) and production (photosynthesis) at Photosystem II (PSII) were monitored using

temperature-controlled oxygen electrode systems maintained at 19°C (Hansatech Instruments). To modulate respiratory activity, salicylhydroxamic acid (SHAM) and antimycin A (AA) (both from Sigma) were added at final concentrations ranging from 400 μM to 2 mM for SHAM, and from 2 to 10 μM for AA.

Measurements with stable isotopes of carbon (^{13}C) and oxygen (^{18}O) in MIMS were performed as described in Fitzpatrick et al. (2022). Cells were taken at around 2.0×10^6 cells mL^{-1} and concentrated to approximately 10 μg chlorophyll mL^{-1} in darkness. The sample was purged with N_2 to minimise background $^{16}O_2$ before a bubble of $^{18}O_2$ (99% Cambridge Isotope Laboratories Inc.) was loaded into the stirring liquid, bringing the concentration of the heavier isotope up to approximately 500 μM. ^{13}C bicarbonate was added to 10 mM concentration. The conversion to $^{13}CO_2$ was enhanced by adding a small volume of Carbonic Anhydrase (Sigma) at 1 mg mL^{-1}. Data were recorded in darkness and later at 25 and 250 μmol photons $m^{-2}\,s^{-1}$. Measurements were performed for 5 min at each light condition. Fluxes were calculated with equations described in Beckmann et al. (2009), which include offsets for the changing relative concentrations of $^{16}O_2$ and $^{18}O_2$.

2.7 | Fluorescence and Spectroscopic Characterisation of Photosynthetic Light Reactions

Chlorophyll fluorescence was imaged in 100 μL of cell suspension placed on a 96-well plate. Cells were dark-adapted for 10 min before measurement. Fluorescence was quantified using a Speedzen III fluorescence imaging setup (JBeam Bio). Maximum fluorescence was determined during the application of saturating red light pulses (250 ms, 3000 μmol photons $m^{-2}\,s^{-1}$), either in the dark (yielding F_m) or during actinic light exposure at 900 μmol photons $m^{-2}\,s^{-1}$ (yielding F_m'). Fluorescence was detected using short blue (470 nm) detection pulses (10 μs). The chlorophyll fluorescence was then measured before (F_0) and during the saturating pulse (F_m), and the electron transfer rate (ETR) was calculated as $(F_m' - F)/F_m' \times \mathrm{PAR} \times 0.5$, where PAR is the intensity of actinic light used to stimulate photosynthesis and the term 0.5 represents 50% of the probability that one electron goes to PSII (instead of PSI).

In vivo spectroscopic analysis was performed with a JTS-10 spectrophotometer (Biologic), equipped with a white LED source filtered through appropriate interference filters, and BG39 filters to protect the photodiodes. The filtered white LED served exclusively as a measuring beam, while photosynthetic changes, including variations in the proton motive force (pmf) revealed by the electro chromic shift (ECS) at 520–545 nm, were monitored. This difference disentangles ECS signatures from spurious changes associated with either cytochrome b6f complex activity (Joliot and Joliot 1994) or with the 535 nm shift that reflects a modification of the xanthophyll diatoxanthin during the onset (or relaxation) of NPQ (Blommaert et al. 2021).

The amplitude of the ECS signal was normalised to a signal corresponding to 1 charge separation, that is, the amplitude induced 150 μs after exposure to saturating single turnover laser flashes. Because PSII was inactivated by the addition of saturating amounts of the inhibitors DCMU (20 μM) and hydroxylamine (1 mM), only PSI is active in these conditions, and therefore, the ECS amplitude corresponds to one charge separation per photosynthetic electron transfer chain (Bailleul et al. 2010).

2.8 | Metabolite Analysis

Metabolites were extracted and analysed as described in Villanova et al. 2017. Ten million cells were harvested on a Durapore-HV membrane filter disc 2.5 cm in diameter and with a pore size of 0.45 μm (Millipore) by vacuum filtration. The filter with the cells was then transferred into a 1.5 mL tube and frozen in liquid nitrogen. Frozen samples were stored at −80°C until metabolite extraction. Metabolites were extracted by immersing the filter in 1 mL of 90% (v/v) methanol containing 0.1 μg mL^{-1} U ^{13}C sorbitol as an internal standard. The tubes were sonicated in a water bath-type sonicator for 1 min in ice-cold water and then incubated at 4°C for 1 h with shaking. The remaining solution was centrifuged at 22000 *g* for 5 min at 4°C. A 50 μL aliquot of the supernatant was used to determine chlorophyll concentration, while a 900 μL aliquot was reduced to dryness using a SpeedVac vacuum concentrator (Thermo Fisher Scientific). Samples were derivatised by adding 40 μL of methoxyamine hydrochloride (20 mg mL^{-1} in pyridine), which was used to resuspend the metabolites by shaking for 2 h at 37°C. Subsequently, 70 μL of MSTFA (prepared by mixing 1 mL MSTFA with 20 μL FAME mix) was added, followed by an additional 30-min incubation with shaking at 37°C. The resulting supernatant was transferred to GC sample vials for GC–MS analysis. Chromatograms and mass spectra were analysed using ChromaTOF software. Metabolite identification was manually verified using the mass spectra and retention indices from the Golm Metabolome Database. Peak intensities of mass fragments were normalised based on the fresh weight of the sample and the quantity of the internal standard (ribitol) added. Statistical differences between groups were assessed using Student's *t*-test on raw data, with significance defined as $p < 0.05$. Relative metabolite levels were calculated as the ratio of each line to the mean value of the corresponding wild-type (WT).

2.9 | Statistical Analysis

For all statistical analyses, unpaired *t*-tests with Welch's correction were performed using GraphPad Prism (version 10.4.1 for Mac OS X, GraphPad Software, Boston, Massachusetts, USA, www.graphpad.com). Statistical significance was denoted as follows: $^*p < 0.05$, $^{**}p < 0.01$ and $^{***}p < 0.001$.

3 | Results

3.1 | Identification of a Putative Transporter Involved in Chloroplast-Mitochondria Energetic Interactions

While previous functional studies in diatoms support the existence of energy exchange between plastids and mitochondria, the molecular components mediating this interaction remain

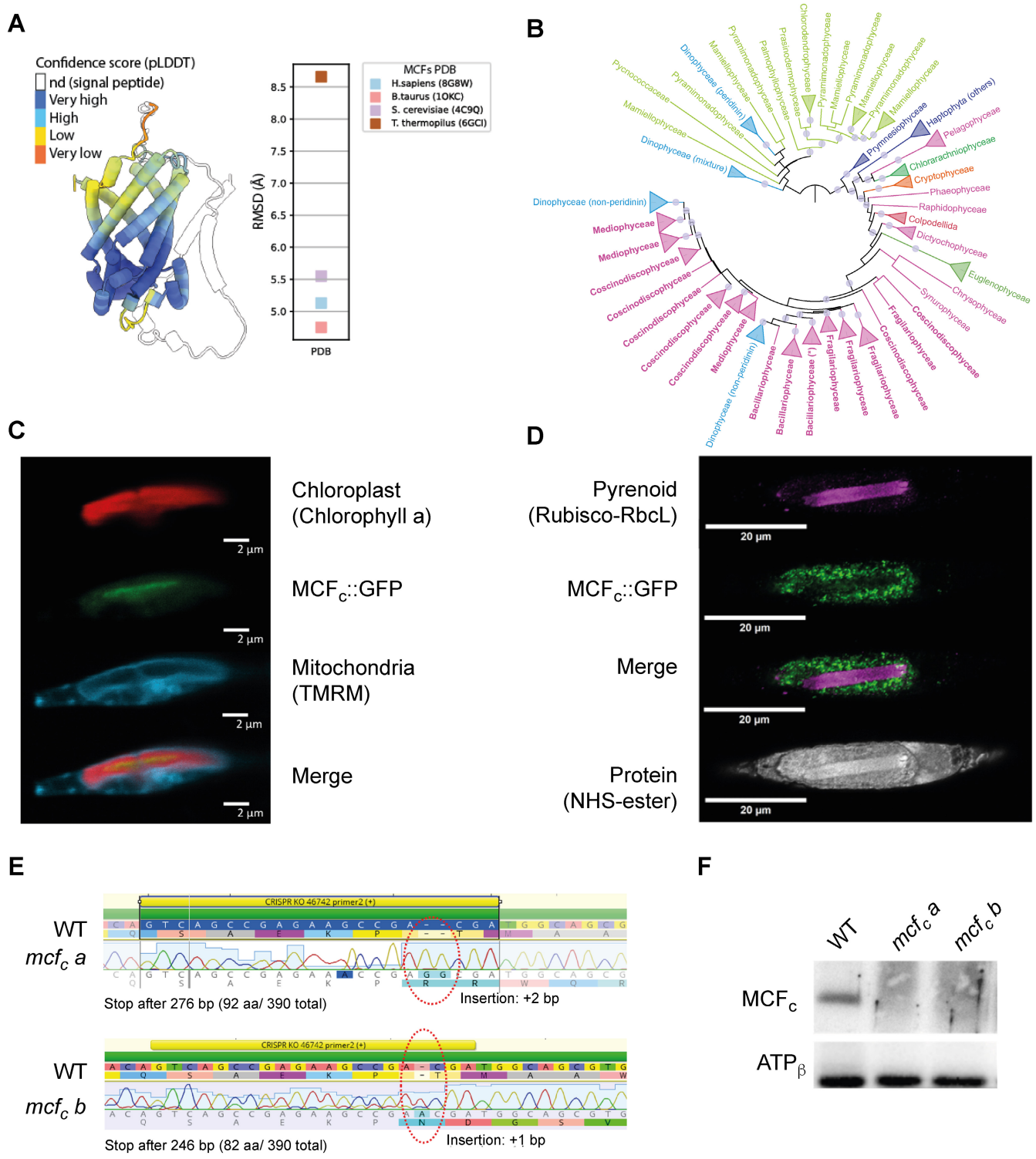

FIGURE 1 | Legend on next page.

unknown. We explored potential players in this process, and identified a candidate MCF transporter, hereafter referred to as MCFc (Phatr3_J46742, also PTI_11G01630 in Pico-PLAZA 3 and PTI_11G01280 in Pico-PLAZA 2), predicted to be plastid-targeted and potentially involved in the exchange of ATP or reducing equivalents across organellar membranes. According to the Ensembl Protists Gene Browser (protists.ensembl.org), Phatr3_J46742 is located on Chromosome 11 and encodes the protein B5Y3N0 (UniProt). The structure of MCFc has been modelled with high confidence in the AlphaFold database (Varadi et al. 2024) (Figure 1A and Figure S1).

We performed a 3D structural homology search using the PDB repository and AlphaFold DB (van Kempen et al. 2024), revealing clear similarities to four well-characterised mitochondrial transporters in mammals and fungi. This approach, along with its classification within the MCF family, suggests that MCFc may transport amino acids, carboxylic acids, fatty

FIGURE 1 | MCFc, a chloroplastic mitochondrial carriers family. (A) Predicted structure of MCFc and its root-mean-square deviation from canonic MCF (B) Phylogenetic tree of MCFc inferred under the C20 model. Monophyletic groups are collapsed at the family level and coloured by taxonomic affiliation (light green: green algae, darker greens: chlorarachniophytes and euglenids, orange: cryptophytes, violet: haptophytes, pink: ochrophytes, blue: dinophytes, red: colpodellids). Diatoms are shown in boldface and the group including Phaeodactylum MCFc (Phatr3_J46742) is denoted by an asterisk (*). Nodes with ultrafast bootstrap support (UFBS) ≥ 85% are indicated by a semi-transparent circle. (C) Subcellular localisation of MCFc. The MCFc-GFP fusion protein colocalises with chlorophyll autofluorescence, but not with mitochondrial markers, indicating plastid localisation. (D) Ultrastructure Expansion Microscopy (U-ExM) confirms the localisation of MCFc within the plastid while excluding its presence in the pyrenoid. The use of NHS-ester staining reveals the total protein content, allowing visualisation of the overall cell morphology. Note the difference in scale bars: Panel (D) shows an expanded cell (scale bar = 20 μm), whereas Panel (C) is unexpanded (scale bar = 2 μm). (E) Molecular characterisation of MCFc KO mutants. Sequencing of Mcf c gene in mcf-a and mcf-b indicates that both clones bear a stop codon after 90 codon triplets due to the insertion of 2 and 1 base pairs, respectively. (F) Western blot analysis confirms the successful knocking out of the Pt-MCF gene by revealing the absence of a specific protein at around 40 kDa in the two mutant lines, ATPβ is the loading control.

acids, cofactors, inorganic ions or nucleotides (Ruprecht and Kunji 2020). Based on its structural similarity to known plastid-targeted MCF transporters such as the land plant ADNT1 for ADP/ATP exchange and an arginine transporter (BAC1), both from *Arabidopsis thaliana* (Table S1; Figures S3 and S4), MCFc appears to be a plastidial protein that potentially plays a role in chloroplast–mitochondria crosstalk.

To address the evolutionary origin and taxonomic distribution of MCFc, close homologues were analysed using a dataset of orthologous groups inferred from high-quality proteomes (Van Vlierberghe, Philippe, and Baurain 2021). The corresponding orthogroup (OG0001460) included three sequences from *P. tricornutum*. A preliminary phylogenetic tree (C20 model, Figure S1A) showed that one gene copy (PTI_10G03480 = Phatr3_J46612, putative mitochondrial copy) belongs to a large group containing both photosynthetic (PS) and non-PS lineages (UFBP support 76%). Another copy (PTI_01G05580 = Phatr3_J42874) is specific to PS heterokonts (=ochrophytes) (UFBS 89%), whereas the third copy (PTI_11G01280 = Phatr3_J46742 = MCFc) lies in a large group that includes many, but only, PS lineages, among which are basal green algae but no land plants or red algae (UFBS 70%). Finally, many diatoms (except *Phaeodactylum*) and a few other lineages displayed a fourth copy, which was provisionally considered as mitochondrial too (UFBS 55%).

The two other PS subtrees (clan OG0001460-8) were then enriched with high-quality transcriptome sequences from PS lineages (Van Vlierberghe, Di Franco, et al. 2021) to clarify the phylogenetic environment of the diatom MCFc gene, yielding a relatively well-supported tree (C20 model, Figure S1B). Ochrophytes were split into two distinct groups, corresponding to the two remaining gene copies of *Phaeodactylum*, with diatoms each time forming a maximally supported monophyletic group (UFBS 96–100%). This prompted us to root the tree on the ochrophyte-specific copy. Similarly, haptophytes were split into two (unequal) groups, but both coincided with the gene copy found in most PS lineages. In the large PS subtree, cryptophytes non-robustly (UFBS 25–55%) appeared near the base of a densely sampled group of red complex algae (i.e., ochrophytes, colpodellids), thus supposedly exhibiting a 'red copy', even though the highly supported (UFBS > 90%) nested positions of complex green euglenids and chlorarachniophytes may seem odd. Surprisingly, most haptophytes grouped with green algae rather than with this red copy. Moreover, the positions of dinophytes showed strong evidence (UFBS > 90%) of lateral gene transfer (LGT) from either ochrophytes (non-peridinin plastids) or, more strangely, from green algae (both peridinin and non-peridinin plastids). Finally, a third inference focusing on the MCFc subtree alone was built to further analyse those relationships while minimising potential reconstruction artefacts (Felsenstein 1978; Gouy et al. 2015). In this well-supported tree (Figure S1B,C), we chose to use green algae as the outgroup, in line with the relatively long branch (UFBS 99%) separating their 'green copy' from the putative red copy of all complex algae. Most relationships remained unchanged in this last analysis, but the evolutionary interpretations are different (see Section 4).

Subcellular localisation studies using an MCFc::GFP fusion revealed co-localisation with chlorophyll autofluorescence (Figure 1C) and with the chloroplastic protein PsbA (Figure S2), but not with mitochondria (Figure 1C). The GFP signal was distributed throughout the plastid, with a notably stronger signal observed near the pyrenoid region. This apparent enrichment may result from the lower chlorophyll autofluorescence in the pyrenoid, which typically interferes with GFP detection elsewhere in the chloroplast but allows clearer visualisation in this zone of reduced chlorophyll. Consistently, expansion microscopy (u-ExM), which removes chlorophyll during sample preparation, revealed a homogenous GFP distribution across the chloroplast with no overlap with Rubisco (Figure 1D), the main component of the pyrenoid. Although fluorescence imaging showed an apparent fluorescence enrichment near the pyrenoid, it likely reflected an envelope-associated signal located above the pyrenoid, where reduced chlorophyll autofluorescence allows enhanced detection. These observations support the hypothesis that this MCF member belongs to a peculiar subfamily that is targeted to the plastid.

3.2 | Generation of MCFc Knockout Mutant Strains

To investigate the potential role of MCFc in chloroplast-mitochondria interactions, we generated knockout (KO) strains using CRISPR-Cas9 technology (Giustini et al. 2024). After transformation, zeocin-resistant *P. tricornutum* (Pt1) colonies were sequenced, revealing two independent clones with mutations in the Phatr3_J46742 gene (MCFc). These mutations introduced a stop codon after 90 or 82 amino acids due to the insertion of 2 and 1 base pair(s), respectively (Figure 1E).

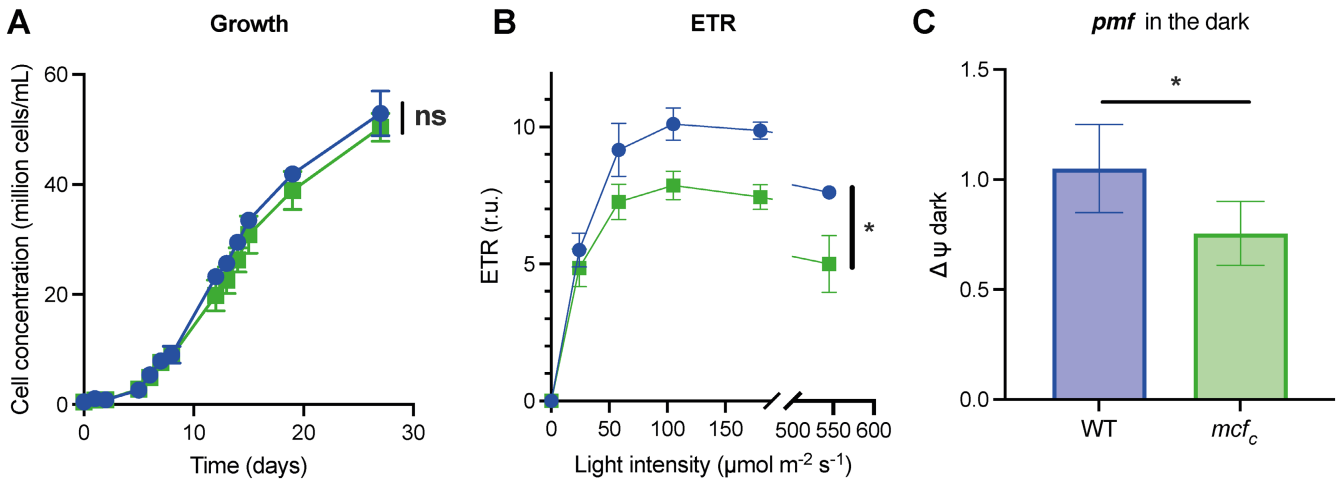

FIGURE 2 | MCFc impacts photosynthesis with no consequence on growth. In blue, the WT; in green, mcf_c. (A) Growth of *Phaeodactylum tricornicum* in autotrophic condition with moderate light regime (12 h/12 h light cycle, 50 µmol photon $m^{-2} s^{-1}$) has been done for the WT and mutant mcf_c. Data ± SD from 6 biological replicates. (B) Photosynthetic efficiency (plotted as ETR) has been measured by chlorophyll fluorescence at different light intensities for the WT and mcf_c. Data ± SD from six biological replicates. (C) The proton motive force (pmf) and especially its $\Delta\Psi$ component has been calculated using the electro chromic shift (ECS) signal measurements. Data ± SD from 6 biological replicates. See methods for more details.

We confirmed the absence of the MCFc protein by immunodetection analysis using a custom-made antibody that recognised a 40 kDa band in the WT, corresponding to the predicted molecular weight of the MCFc protein. This band was absent in the mutant lines, confirming the successful generation of KO lines for the Phatr3_J46742 gene (Figure 1F).

We explored the potential role of MCFc in diatom energetics, monitoring the growth and photosynthetic capacity of the two KO mutant strains. We combined the results from both clones because their phenotypes were indistinguishable. Although no growth defects were observed (Figure 2A and Figure S5A), we found that the KO lines had lower photosynthetic performance (electron transport rate [ETR]) compared to WT cells (Figure 2B; Figure S5B and Table S2). To complete the physiological characterisation of the mutants, we assessed their ability to maintain a pmf ($\Delta\Psi d$) in the dark, a functional trait revealing the chloroplast-mitochondria interactions (Bailleul et al. 2015). This parameter was quantified using the Electrochromic Shift (ECS) signal, which responds to changes in membrane $\Delta\Psi$ with linear (at 520 nm) and quadratic (at 565 nm) dependencies (Bailleul et al. 2015; Joliot and Joliot 1989). The $\Delta\Psi d$ signal was approximately 25% lower in the mutant strains compared to the WT (Figure 2C and Figure S5C), indicating that MCFc contributes to energy interactions between these two organelles. However, this role appears to be partial and is likely complemented or compensated by other metabolic exchanges, which may help to mitigate the impact of MCFc disruption.

3.3 | MCFc Modulates the Relationship Between Photosynthesis and Respiration

We monitored the relationship between oxygen production (from water-splitting in PSII) and oxygen consumption (via respiration) (Figure 3A and Figure S6A). In diatoms, these processes are linearly correlated, suggesting the existence of a link between the export of excess reducing power from the plastid to the mitochondria, its use for ATP production, and the subsequent import of ATP into the chloroplast to drive CO_2 assimilation (Bailleul et al. 2015). Since MCFc may influence photosynthetic ETR and the membrane potential in the dark ($\Delta\Psi d$) as part of the pmf, we examined the interplay between photosynthesis and respiration under varying concentrations of SHAM and Antimycin A, two inhibitors of mitochondrial respiration that gradually reduce mitochondrial activity. We observed a linear relationship between the two mechanisms (respiration and photosynthesis) in WT cells (Figure 3A and Figure S6A), indicating that increased activity in one process enhances the other. This result aligned with previous findings (Bailleul et al. 2015). The linear relationship observed here was preserved in the absence of MCFc, although the slope of oxygen evolution versus consumption was less steep (Figure 3A and Figure S6A), suggesting that organelle crosstalk was weakened.

We corroborated these findings using the more specific membrane inlet mass spectrometry (MIMS) technique (reviewed in Burlacot et al. 2020). MIMS is particularly well-suited for detecting dynamic, short-term effects, such as alternative flows through less efficient transporters driven by elevated substrate concentrations, often obscured under steady-state conditions by compensatory mechanisms. By employing ^{18}O and ^{13}C isotopes, we simultaneously recorded PSII O_2 evolution and cellular respiration rates under varying light conditions. Photosynthetic O_2 evolution and $^{13}CO_2$ fixation rates followed a similar trend in the mutant and WT strains, showing an approximately linear relationship with light intensity. However, the $^{18}O_2$ uptake rate increased sharply under high-light conditions in the mutant (Figure 3B,C and Figure S6B,C).

Additionally, the oxygen uptake of the mcf_c strain exhibited a brief spike (lasting about 10 s) after transitioning to high light before stabilising at a lower steady-state uptake, suggesting a transient accumulation of undefined respiratory substrates due to the absence of the MCFc transporter. Overall, the O_2 evolution-to-uptake ratio was significantly lower in the mcf_c mutant

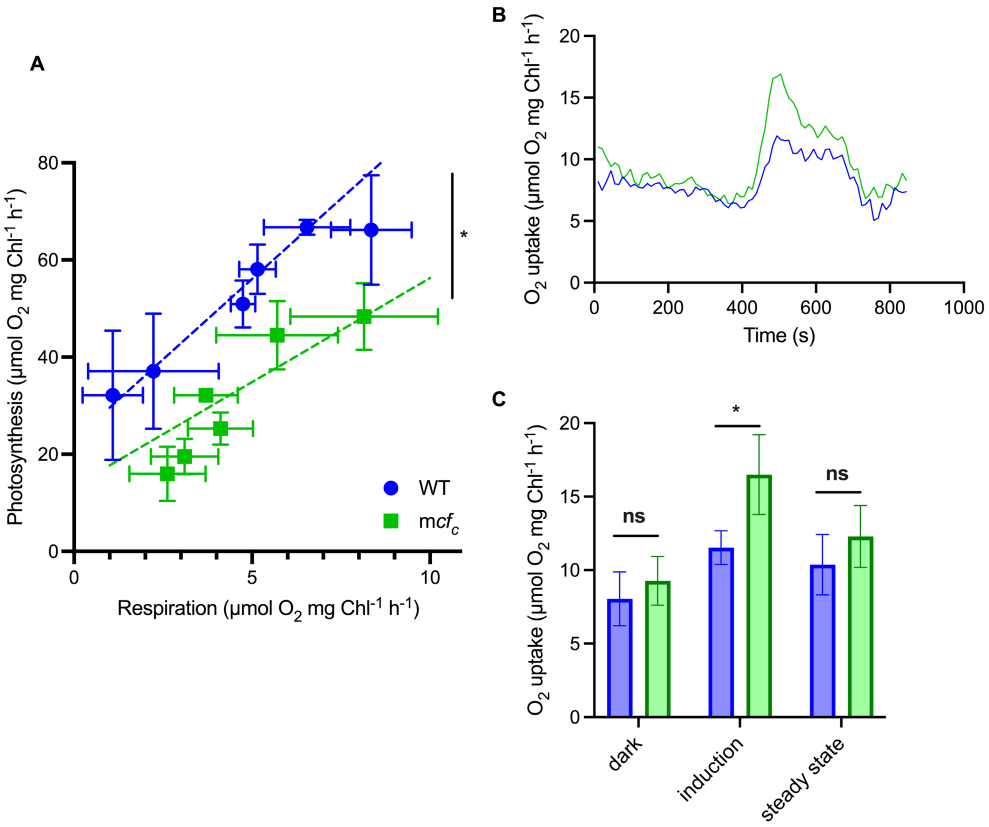

FIGURE 3 | Analysis of the photosynthesis/respiration relationship. In blue, the WT, in green *mcf*$_c$. (A) In *P. tricornutum* cells collected in the exponential growth phase, photosynthetic activity was measured as O_2 evolution (in the light), while respiration is the rate as O_2 uptake in the dark. Data ± SD from six biological replicates. Datapoints refer to the following concentrations of salicylhydroxamic acid (SHAM) and Antimycin A (AA), respectively: 0 (control); 400 + 2 µM; 660 + 3.33 µM; 1 mM + 5 µM; 1.33 mM + 13.3 µM and 2 mM + 10 µM. (B, C) O_2 uptake rates measured by membrane inlet mass spectrometer (MIMS) in presence of ^{18}O-labelled O_2 representative traces shown in (B). Cells were dark-adapted before the experiment. Black bars indicate the dark period, white bars the light period. (C) Average ±SD of four independent replicates extracted from (B).

compared to the WT under high light conditions (Figure 3B,C and Figure S6B,C), explaining the differential slope observed in Figure 3A. Based on the notion that MCFc is involved in energy exchanges between the chloroplast and mitochondria, this transient increase in O_2 consumption might indicate increased respiration activity due to an over-reduction of PSII.

3.4 | Metabolite Analysis-Based Analysis of Chloroplast-Mitochondria Exchanges

To investigate the nature of the metabolite(s) exchanged through MCFc. We performed a comparative metabolomics analysis. The absence of MCFc resulted in a significant decrease in several amino acids, including aspartic acid (Asp), glutamic acid (Glu), asparagine (Asn), leucine (Leu) and 2-ketoglutarate (2-KG, the precursor of Glu). In contrast, arginine (Arg) levels were elevated in the mutant compared to the WT (Figure 4 and Table S3).

3.5 | In Silico Analysis of MCFc Putative Structure and Substrate Specificity

The transport mechanism of mitochondrial ADP/ATP carriers is well described and likely generalisable to other mitochondrial carriers (Ruprecht and Kunji 2020; Palmieri and Pierri 2010). These carriers typically have a single substrate-binding site and two substrate recognition gates on each side of the membrane (Figure S7). The coordinated movement of six transmembrane (TM) helices facilitates the alternating opening and closing of the matrix or intermembrane space (confluent with the cytosol), preventing proton leakage from the lumen. The coupling between TM helices 1–2, 3–4 and 5–6 is driven by interactions between similar sequence motifs that complement the joint TMs within the doublets, conferring substrate specificity (Ruprecht and Kunji 2020).

An analysis of the corresponding motifs in MCFc homologs, based on structural alignment and motif scoring (Figure S7), revealed that the odd-numbered TM helices (1, 3 and 5) share very similar motifs. At the same time, this pattern did not hold for the even-numbered TMs, suggesting a potentially different structural mechanism. By evaluating MCFc similarity to known MCF proteins, possible substrates could include aspartate/glutamate, ATP-Mg/Pi or citrate (Table S1).

4 | Discussion

In this work, we sought to identify potential factors that influence the optimal dialogue between organelles in diatoms. These organisms, which represent the complex red lineage of

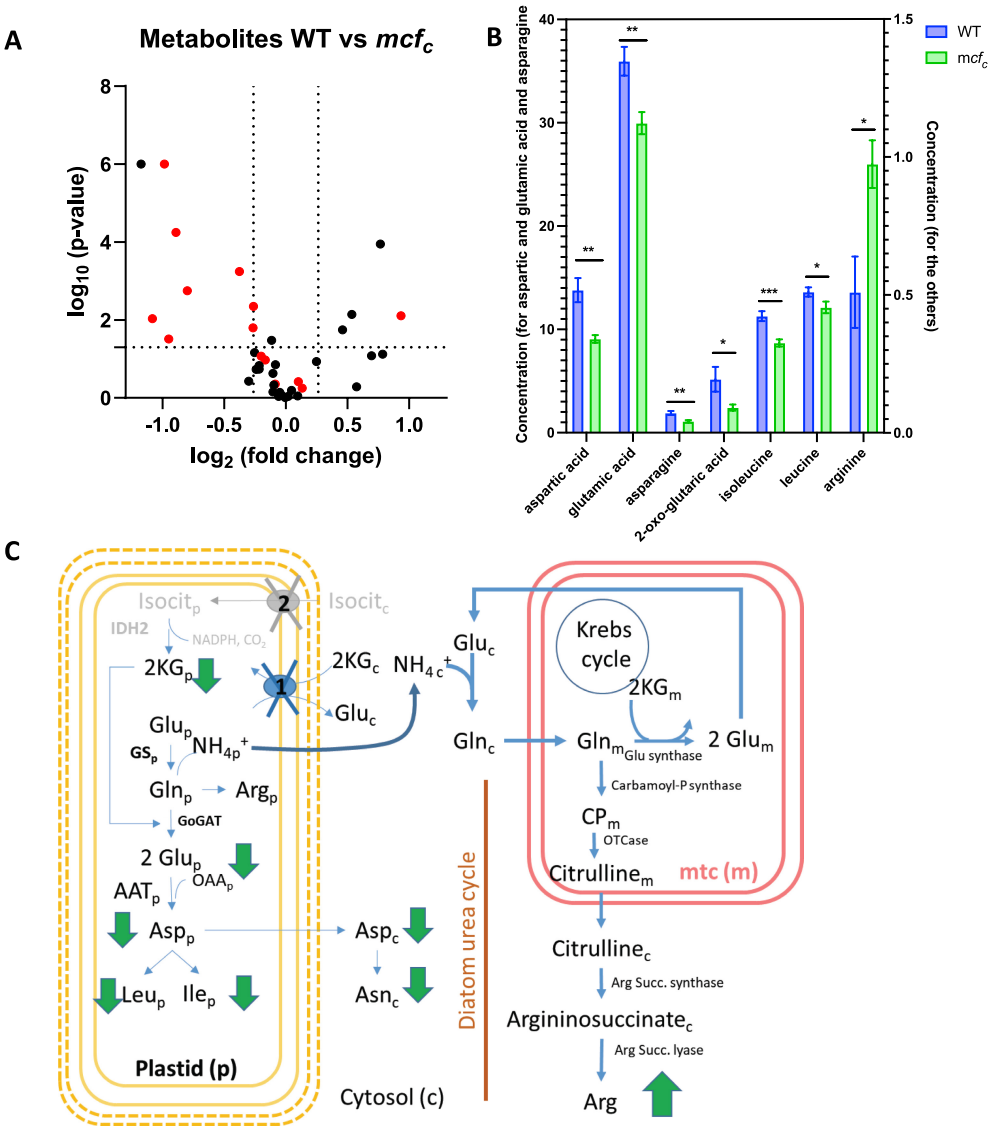

FIGURE 4 | Metabolic flexibility. (A) Volcano plot showing the differential concentration of metabolites in mcf_c relative to the WT (the amino acids group is in red). (B) Amino acid concentration in WT and mcf_c. Data ± SD from at least six biological replicates. (C) Schematic representation of metabolite changes in *P. tricornutum* cells. Flux changes upon mutagenesis are highlighted by green arrows.

phototrophs, share the most fundamental characteristics of oxygenic photosynthesis found in primary algae. However, a complete understanding of the molecular components responsible for optimising the photosynthesis process in diatoms remains incomplete.

4.1 | Optimising ATP/NADPH Stoichiometry and Strategies

Photosynthesis relies on maintaining an optimal ATP/NADPH ratio, which is established during the light reactions. This balance is typically regulated by adjusting the contributions of linear and alternative electron flow processes. One mechanism involves the export of reducing equivalents from the plastid to mitochondrial oxidases (Kinoshita et al. 2011). This process enables mitochondria to support photosynthetic activity under specific conditions and has been observed in green plants, with particularly high activity in some microalgae.

For instance, KO strains with double mutations in respiratory complexes (Cardol et al. 2009; Lemaire et al. 1988) exhibit severe growth defects, underscoring the critical role of mitochondrial function in green algae such as *Chlamydomonas*. Remarkably, the *Chlamydomonas* mutant strain Fud50su, which lacks the plastidial ATP synthase, can restore phototrophic growth in a revertant strain. This recovery is achieved through enhanced ATP import from mitochondria via the ATP/ADP transporter (Merchant et al. 2007; Lemaire et al. 1988), highlighting the interplay between plastids and mitochondria energy metabolism.

In diatoms, direct energetic exchange plays a crucial role (Bailleul et al. 2015; Murik et al. 2019). Computational simulations and experimental analyses suggest that organelle crosstalk plays a key role in regulating light-dependent metabolic changes in these organisms (Prihoda et al. 2012). In addition to direct metabolic exchanges, several 'indirect' interactions between organelles have also been well documented. For instance, CO_2 produced by oxidative phosphorylation can be immediately refixed

in the plastid (Busch et al. 2013; Riazunnisa et al. 2006), O_2 generated by photosynthesis can be consumed by mitochondria before diffusing out of the cell (Lavergne 1989), and functional studies in *Arabidopsis* suggest that H_2O_2 accumulation can trigger coordinated responses between plastids and mitochondria to relieve PSI acceptor-side limitations (Fitzpatrick et al. 2022). Consistent with this possibility, increased light-dependent respiratory CO_2 evolution was seen when infiltrating Arabidopsis plants with Methyl viologen (MV). These experiments were consistent with a possible H_2O_2 priming of mitochondria to accept excess energy, potentially through the malate shuttle. The MCFc mutations generated in this work affect both photosynthesis (Figure 2) and respiration (Figure 3). Thus, they alter the relationship between these two processes in mutant cells (Figure 3A).

4.2 | Molecular Players Involved in Organelle Exchanges in Diatoms

Despite functional studies (Bailleul et al. 2015), and modelling approaches (Levering et al. 2016; Broddrick et al. 2019), the molecular mechanisms governing plastid-mitochondria interactions in diatoms and complex red plastids in general remain poorly understood. Previous research has identified bacteria-like plastidial nucleotide transporters (NTTs) in diatoms, which are localised in the plastid envelope (Ast et al. 2009; Gruber and Haferkamp 2019). These transporters may play a role in supplying nucleotides to the plastid for energy metabolism, but their exact energetic role is unclear, as they do not catalyse ATP/ADP exchange like in primary plastids (Ast et al. 2009; Chu et al. 2017).

Several other diatom transporters localised to the thylakoid or envelope membranes have been studied (reviewed in Marchand et al. 2018; Finazzi et al. 2015; Carraretto et al. 2016). These transporters primarily include carriers of ions and a limited number of metabolites. However, their known activities and substrate specificities do not align with the functions investigated in this study.

Bioinformatic, molecular and physiological analyses suggest that MCFc is a member of the MCF group. Moreover, confocal imaging of GFP-tagged strains confirms that Phaeodactylum MCFc is specifically targeted to the plastid, as are Arabidopsis ADNT1 and BAC1. Yet, in terms of sequence homology, MCFc is distant from both these plastid-targeted MCF transporters, since the three proteins were recovered in different orthogroups (clans OG0001460-8, OG0000089-40 and OG0000128-21, respectively) by Van Vlierberghe, Philippe, and Baurain (2021), each group containing closer homologs from non-PS organisms (e.g., Figure S1A). Whereas MCFc orthologues are widespread in complex algal lineages, whether equipped with a red or a green plastid, they are much scarcer in primary algae (Figure 1B,C), with no representative in glaucophytes (apparently), red algae or beyond basal green algae (i.e., Prasinodermophyta, 'prasinophytes' and Chlorodendrophyceae). This observation suggests either early parallel losses of the primary gene after endosymbiotic transfer of the red copy to complex algae or recruitment from a non-primary source. Regarding the second possibility, there exists a close paralogous copy of MFCc (Phatr3_J42874) that is specific to ochrophytes and might be at the origin of MCFc in all complex algae (Figure S1B). In any case, many gene transfers are needed to explain the distribution and phylogeny of MCFc sequences reported in this work, for example, in complex green algae and in multiple types of dinophytes. A recruitment of MFCc from another compartment after duplication, as proposed for several key genes such as the plastid-targeted GAPDH (GapC-I) of complex red algae, initially of cytosolic origin (Harper and Keeling 2003; Petersen et al. 2014; Van Vlierberghe, Di Franco, et al. 2021), seems implausible here (see the legend of Figure S1 for more discussion).

While its precise substrate remains unidentified, the deletion of MCFc significantly impacts the accumulation of the key amino acid precursor 2-KG (α-ketoglutarate) and other amino acids. This disruption is likely due to impaired partitioning of aspartate, glutamate, asparagine, and arginine between the plastid and cytosol. Our analysis suggests different hypotheses to explain its function (Figure 4C).

Hypothesis 1, (Figure 4C: *MCFc transports 2-KG inside the plastid* [maybe against glutamate]). Indeed, the reduced levels of Glu and 2-KG in the mutant likely originate from the chloroplast, which is about 10 times larger than the mitochondrion (Uwizeye et al. 2021). Usually, nitrogen fixation occurs in the plastid through the combined action of glutamine synthetase and GOGAT, but de novo 2-KG synthesis happens exclusively in the mitochondrion. Therefore, our first hypothesis would be that 2-KG import into the plastid of the MCFc mutant is hindered, which could account for the decreased Glu synthesis. Since Glu is required for Asp production, a reduction in Glu would lower Asp concentrations in the plastid (AspP in Figure 4C), assuming amino acid demand is maintained and subsequently reduces amino acids derived from Asp, such as Leu, isoleucine (Ile) and Asn (following AspP export).

As a result, nitrogen fixation in the MCFc mutant may rely more heavily on cytosolic glutamine synthase, given the reduced utilisation of NH_4^+ in the plastid due to decreased 2-KG availability and the diffusion of NH_4^+ from the plastid. The interplay between nitrogen and carbon metabolism indicates that carbon is essential for nitrogen assimilation and vice versa (Smith et al. 2019; Obata et al. 2013; Huppe and Turpin 1994). Consequently, excess nitrogen in the cytosol could be redirected towards Arg synthesis via cytosolic glutamine synthase and potentially towards a hypothesised urea cycle in diatoms (Allen et al. 2011), which also involves arginine (as shown in the lower right of the scheme). These adjustments align with the need for nitrogen to sustain photosynthetic processes while maintaining carbon assimilation. These changes would explain the significant increase in cytosolic Arg, the most prominent difference observed among the metabolites analysed (Figure 4C, Hypothesis 1), and account for the lower functional effect of the mutation in nitrogen-limited conditions.

Hypothesis 1 can explain (1) a lower ETR (decreased electron sink in the plastid), (2), metabolomics data (see above), (3) MIMS results (default in 2-KG import into the plastid would reroute this metabolite towards complete respiration in the TCA cycle) and (iv) it would be consistent with in silico predictions. In land plants, oxoglutarate/glutamate exchange is carried out by the combined action of DIT1 ($2\text{-}KG_{in}/malate_{out}$) and DIT2

($glutamate_{out}$/$malate_{in}$), resulting in no net malate transport but net export of fixed nitrogen. The ortholog of DIT1 in *P. tricornutum* encoded by Phatr3_EG02645, shares domain homology with the Arabidopsis DIT1 2-oxoglutarate-malate exchanger. However, the gene model lacks an ER transit peptide signal and the diatom plastid targeting signal (Gruber et al. 2007). Additionally, the occurrence of plastid-localised enzymes in *P. tricornutum* that use malate as a substrate has not been found yet in the genome (Broddrick et al. 2019), raising doubts about DIT1/DIT2 cooperation in diatoms.

While this hypothesis is plausible, although the effect of mutation is diminished in the absence of nitrogen, measurements across different nitrogen levels revealed a similar trend (Figure S7), suggesting that alternative explanations should be considered.

Alternatively, Hypothesis 2, *deficient import of isocitrate into the plastid* (Figure 4C, grey pathways) could also lead to a similar metabolic phenotype, as isocitrate could provide 2-KG via plastidial isocitrate dehydrogenase (ICDH) activity (Huang et al. 2021). A putative substrate suggested by in silico analysis is indeed citrate (Figure S8 and Table S1). Tricarboxylate transporters transport both citrate and isocitrate (Picault et al. 2002), but citrate does not have any known documented metabolic role in the plastid of diatoms, nor in land plants. A plastidial isocitrate dehydrogenase (catalysing the reaction isocitrate + NADP+ < − > 2-KG + NADPH + CO_2) has been identified in both land plants (see http://chlorokb.fr) and *P. tricornutum* (Huang et al. 2021). If this plastidial enzyme functions in the direction of isocitrate decarboxylation (Direction 1), then cytosolic isocitrate must be imported into the plastid. This pathway would provide an alternative source of 2-KG for nitrogen assimilation. Defective isocitrate import (isocitrate dehydrogenase operating in Direction 1) could also explain MIMS results and the metabolic profile. The concomitant production of NADPH by isocitrate dehydrogenase—apparently unnecessary in the plastid during the light phase—may explain why the role of this enzyme is not yet fully understood. However, if the isocitrate dehydrogenase works in the carboxylation direction (Direction 2, 2-KG + NADPH + CO_2 − > isocitrate + $NADP^+$), it could serve as a mechanism to alleviate redox pressure in the plastid and provide isocitrate to the cytosol for lipid synthesis. Regardless of the direction in which the enzyme operates, isocitrate transport across the plastid envelope is essential, although no such transporter has yet been identified.

Finally, in silico comparative analysis of the MCFc predicted structure suggests that another possible substrate (Hypothesis 3) could be ATP (Table S1 and Figure S8). Changes in the pmf observed in the dark would be consistent with this hypothesis. However, the lower dark plastidial pmf might be an indirect consequence of metabolic perturbation, such as a lower pH in the stroma due to modified abundant amino acid concentrations.

In conclusion, this study underscores the intricate nature of intracellular metabolite transport and its connection to energy metabolism in diatoms. Although many key molecular players remain elusive, our integrated approach—encompassing molecular biology, bioinformatics and physiology—provides valuable insights and lays a strong foundation for advancing our understanding of these unique organisms in the years to come.

Author Contributions

Conceptualisation: Giovanni Finazzi. Coordination: Giovanni Finazzi, Gilles Curien, Alisdair R. Fernie, Pierre Cardol, Denis Baurain, Eva-Mari Aro and Dimitri Tolleter coordinated the research. Experiments: Cécile Giustini, Davide Dal Bo, Mattia Storti, Mick Van Vlierberghe, Denis Baurain, Youjun Zhang, Duncan Fitzpatrick, Guillaume Allorent, Pascal Albanese and Dimitri Tolleter performed the experiments. Manuscript writing: Giovanni Finazzi and Dimitri Tolleter drafted the manuscript with contributions from all authors. Review and approval: All authors reviewed and approved the final manuscript.

Acknowledgements

We thank Richard Dorrell for kindly providing the MCFc::GFP mutant, Luigi and Ferdinando Palmieri for their helpful discussions and efforts on MCFc transporter assays and Chris Bowler for fruitful discussion in the initial phase of the project. C.G., G.C., M.S., D.T. and G.F. acknowledge funding from the European Research Council ERC (Chloro-Mito; grant no. 833184). P.A. acknowledges funding from the European Union's Horizon 2020 Research and Innovation Program under the Marie Skłodowska-Curie grant agreement No 101066400; PHOTO-LINK. G.F. acknowledges funds from the Plankton Project (grant agreement 101099192). G.A. and E.-M.A. acknowledge funding from the CNRS Momentum Program and the Jane and Aatos Erkko Foundation, respectively. Data are available at Giovanni Finazzi (giovanni.finazzi@cea.fr) and Dimitri Tolleter (dimitri.tolleter@cea.fr). We confirm that no generative AI tool was used to create or interpret research content, data or analysis in this manuscript. We used Grammarly software only to assist in refining language, readability and clarity of the manuscript text. All intellectual content and final wording were reviewed and approved by the authors.

Data Availability Statement

The data that support the findings of this study are available from the corresponding author upon reasonable request.

References

Allen, A. E., C. L. Dupont, M. Oborník, et al. 2011. "Evolution and Metabolic Significance of the Urea Cycle in Photosynthetic Diatoms." *Nature* 473, no. 7346: 203–207.

Alric, J. 2010. "Cyclic Electron Flow Around Photosystem I in Unicellular Green Algae." *Photosynthesis Research* 106, no. 1–2: 47–56. https://doi.org/10.1007/s11120-010-9566-4.

Ast, M., A. Gruber, S. Schmitz-Esser, et al. 2009. "Diatom Plastids Depend on Nucleotide Import From the Cytosol." *Proceedings of the National Academy of Sciences of the United States of America* 106, no. 9: 3621–3626.

Bailleul, B., N. Berne, O. Murik, et al. 2015. "Energetic Coupling Between Plastids and Mitochondria Drives CO_2 Assimilation in Diatoms." *Nature* 524, no. 7565: 366–369. https://doi.org/10.1038/nature14599.

Bailleul, B., P. Cardol, C. Breyton, and G. Finazzi. 2010. "Electrochromism: A Useful Probe to Study Algal Photosynthesis." *Photosynthesis Research* 106: 179–189.

Beckmann, K., J. Messinger, M. R. Badger, T. Wydrzynski, and W. Hillier. 2009. "On-Line Mass Spectrometry: Membrane Inlet Sampling." *Photosynthesis Research* 102: 511–522.

Berges, J. A., D. J. Franklin, and P. J. Harrison. 2001. "Evolution of an Artificial Seawater Medium: Improvements in Enriched Seawater,

Artificial Water Over the Last Two Decades." *Journal of Phycology* 1145: 1138–1145.

Blommaert, L., L. Chafai, and B. Bailleul. 2021. "The Fine-Tuning of NPQ in Diatoms Relies on the Regulation of Both Xanthophyll Cycle Enzymes." *Scientific Reports* 11: 12750. https://doi.org/10.1038/s41598-021-91483-x.

Broddrick, J. T., N. Du, S. R. Smith, et al. 2019. "Cross-Compartment Metabolic Coupling Enables Flexible Photoprotective Mechanisms in the Diatom *Phaeodactylum tricornutum*." *New Phytologist* 222, no. 3: 1364–1379. https://doi.org/10.1111/nph.15685.

Burlacot, A., F. Burlacot, Y. Li-Beisson, and G. Peltier. 2020. "Membrane Inlet Mass Spectrometry: A Powerful Tool for Algal Research." *Frontiers in Plant Science* 11: 1302. https://doi.org/10.3389/fpls.2020.01302.

Busch, F. A., T. L. Sage, A. B. Cousins, and R. F. Sage. 2013. "C3 Plants Enhance Rates of Photosynthesis by Reassimilating Photorespired and Respired CO_2." *Plant, Cell & Environment* 36, no. 1: 200–212. https://doi.org/10.1111/j.1365-3040.2012.02567.x.

Cardol, P., J. Alric, J. Girard-Bascou, F. Franck, F. A. Wollman, and G. Finazzi. 2009. "Impaired Respiration Discloses the Physiological Significance of State Transitions in Chlamydomonas." *Proceedings of the National Academy of Sciences of the United States of America* 106, no. 37: 15979–15984. https://doi.org/10.1073/pnas.0908111106. Erratum in: 2019. *Proceedings of the National Academy of Sciences of the United States of America* 116, no. 14: 7150. https://doi.org/10.1073/pnas.1903574116.

Carraretto, L., E. Teardo, V. Checchetto, G. Finazzi, N. Uozumi, and I. Szabo. 2016. "Ion Channels in Plant Bioenergetic Organelles, Chloroplasts and Mitochondria: From Molecular Identification to Function." *Molecular Plant* 9, no. 3: 371–395. https://doi.org/10.1016/j.molp.2015.12.004.

Chu, L., A. Gruber, M. Ast, et al. 2017. "Shuttling of (Deoxy-) Purine Nucleotides Between Compartments of the Diatom *Phaeodactylum tricornutum*." *New Phytologist* 213, no. 1: 193–205.

Felsenstein, J. 1978. "Cases in Which Parsimony or Compatibility Methods Will Be Positively Misleading." *Systematic Zoology* 27: 401–410.

Finazzi, G., D. Petroutsos, M. Tomizioli, et al. 2015. "Ions Channels/Transporters and Chloroplast Regulation." *Cell Calcium* 58, no. 1: 86–97. https://doi.org/10.1016/j.ceca.2014.10.002.

Fitzpatrick, D., E.-M. Aro, and A. Tiwari. 2022. "True Oxygen Reduction Capacity During Photosynthetic Electron Transfer in Thylakoids and Intact Leaves." *Plant Physiology* 189, no. 1: 112–128.

Giustini, C., J. Angulo, F. Courtois, and G. Allorent. 2024. "Targeted Gene Editing of Nuclear-Encoded Plastid Proteins in *Phaeodactylum tricornutum* via CRISPR/Cas9." In *Plastids. Methods in Molecular Biology*, edited by E. Maréchal, vol. 2776. Humana.

Gouy, R., D. Baurain, and H. Philippe. 2015. "Rooting the Tree of Life: The Phylogenetic Jury Is Still out." *Philosophical Transactions of the Royal Society of London. Series B, Biological Sciences* 370: 20140329.

Gruber, A., and I. Haferkamp. 2019. "Nucleotide Transport and Metabolism in Diatoms." *Biomolecules* 9, no. 12: 761. https://doi.org/10.3390/biom9120761.

Gruber, A., G. Rocap, P. G. Kroth, E. V. Armbrust, and T. Mock. 2015. "Plastid Proteome Prediction for Diatoms and Other Algae With Secondary Plastids of the Red Lineage." *Plant Journal* 81, no. 3: 519–528. https://doi.org/10.1111/tpj.12734.

Gruber, A., S. Vugrinec, F. Hempel, S. B. Gould, U. G. Maier, and P. G. Kroth. 2007. "Protein Targeting Into Complex Diatom Plastids: Functional Characterisation of a Specific Targeting Motif." *Plant Molecular Biology* 64, no. 5: 519–530.

Harper, J. T., and P. J. Keeling. 2003. "Nucleus-Encoded, Plastid-Targeted Glyceraldehyde-3-Phosphate Dehydrogenase (GAPDH) Indicates a Single Origin for Chromalveolate Plastids." *Molecular Biology and Evolution* 20: 1730–1735.

Harrison, P. J., R. E. Waters, and F. J. R. Taylor. 1980. "A Broad Spectrum Artificial Sea Water Medium for Coastal and Open Ocean Phytoplankton." *Journal of Phycology* 16, no. 1: 28–35.

Hoefnagel, M. H. N., O. K. Atkin, and J. T. Wiskich. 1998a. "Interdependence Between Chloroplasts and Mitochondria in the Light and the Dark." *Biochimica et Biophysica Acta (BBA)-Bioenergetics* 1366, no. 3: 235–255.

Hoefnagel, M. H. N., O. K. Atkin, and J. T. Wiskich. 1998b. "Interdependence Between Chloroplasts and Mitochondria in the Light and the Dark." *Biochimica et Biophysica Acta - Bioenergetics* 1366, no. 3: 235–255. https://doi.org/10.1016/s0005-2728(98)00126-1.

Huang, S., J. Zhao, W. Li, P. Wang, Z. Xue, and G. Zhu. 2021. "Biochemical and Phylogenetic Characterization of a Novel $NADP^+$-Specific Isocitrate Dehydrogenase From the Marine Microalga *Phaeodactylum tricornutum*." *Frontiers in Molecular Biosciences* 8: 702083.

Huppe, H. C., and D. H. Turpin. 1994. "Integration of Carbon and Nitrogen Metabolism in Plant and Algae Cells." *Annual Review of Plant Biology* 45: 577–607. https://doi.org/10.1146/annurev.pp.45.060194.003045.

Irisarri, I., D. Baurain, H. Brinkmann, et al. 2017. "Phylotranscriptomic Consolidation of the Jawed Vertebrate Timetree." *Nature Ecology & Evolution* 1: 1370–1378.

Joliot, P., and A. Joliot. 1989. "Characterization of Linear and Quadratic Electrochromic Probes in Chlorella Sorokiniana and *Chlamydomonas reinhardtii*." *Biochimica et Biophysica Acta (BBA)-Bioenergetics* 975, no. 3: 355–360.

Joliot, P., and A. Joliot. 1994. "Mechanism of Electron Transfer in the Cytochrome b/f Complex of Algae: Evidence for a Semiquinone Cycle." *Proceedings of the National Academy of Sciences* 91, no. 3: 1034–1038.

Katoh, K., and D. M. Standley. 2013. "MAFFT Multiple Sequence Alignment Software Version 7: Improvements in Performance and Usability." *Molecular Biology and Evolution* 30: 772–780.

Keeling, P. J., F. Burki, H. M. Wilcox, et al. 2014. "The Marine Microbial Eukaryote Transcriptome Sequencing Project (MMETSP): Illuminating the Functional Diversity of Eukaryotic Life in the Oceans Through Transcriptome Sequencing." *PLoS Biology* 12, no. 6: e1001889.

Kinoshita, H., J. Nagasaki, A. Yoshikawa, et al. 2011. "The Chloroplastic 2-Oxoglutarate/Malate Transporter Has Dual Function as the Malate Valve and in Carbon/Nitrogen Metabolism." *Plant Journal* 65, no. 1: 15–26.

Klena, N., G. Maltinti, U. Batman, G. Pigino, P. Guichard, and V. Hamel. 2023. "An In-Depth Guide to the Ultrastructural Expansion Microscopy (U-ExM) of *Chlamydomonas reinhardtii*." *Bio-Protocol* 13, no. 17: e4792. https://doi.org/10.21769/BioProtoc.4792.

Lavergne, J. 1989. "Mitochondrial Responses to Intracellular Pulses of Photosynthetic Oxygen." *Proceedings of the National Academy of Sciences of the United States of America* 86, no. 22: 8768–8772. https://doi.org/10.1073/pnas.86.22.8768.

Le, Q. S., O. Gascuel, and N. Lartillot. 2008. "Empirical Profile Mixture Models for Phylogenetic Reconstruction." *Bioinformatics* 24: 2317–2323.

Le, S. Q., C. C. Dang, and O. Gascuel. 2012. "Modeling Protein Evolution With Several Amino Acid Replacement Matrices Depending on Site Rates." *Molecular Biology and Evolution* 29: 2921–2936.

Lemaire, C., F. A. Wollman, and P. Bennoun. 1988. "Restoration of Phototrophic Growth in a Mutant of *Chlamydomonas reinhardtii* in Which the Chloroplast atpB Gene of the ATP Synthase Has a Deletion: An Example of Mitochondria-Dependent Photosynthesis." *Proceedings of the National Academy of Sciences of the United States of America* 85, no. 5: 1344–1348. https://doi.org/10.1073/pnas.85.5.1344.

Letunic, I., and P. Bork. 2024. "Interactive Tree of Life (iTOL) v6: Recent Updates to the Phylogenetic Tree Display and Annotation Tool." *Nucleic Acids Research* 52: W78–W82. https://doi.org/10.1093/nar/gkae268.

Levering, J., J. Broddrick, C. L. Dupont, et al. 2016. "Genome-Scale Model Reveals Metabolic Basis of Biomass Partitioning in a Model Diatom." *PLoS One* 11, no. 5: e0155038. https://doi.org/10.1371/journal.pone.0155038.

Liu, S., S. M. Yang, C. Bowler, M. Obornik, and R. Dorrell. 2025. "Dynamic Relocalization and Divergent Expression of a Major Facilitator Carrier Subfamily in Diatoms." *Physiologia Plantarum* 177, no. 3: e70355. https://doi.org/10.1111/ppl.70355.

Marchand, J., P. Heydarizadeh, B. Schoefs, and C. Spetea. 2018. "Ion and Metabolite Transport in the Chloroplast of Algae: Lessons From Land Plants." *Cellular and Molecular Life Sciences* 75, no. 12: 2153–2176. https://doi.org/10.1007/s00018-018-2793-0.

Merchant, S. S., S. E. Prochnik, O. Vallon, et al. 2007. "The Chlamydomonas Genome Reveals the Evolution of Key Animal and Plant Functions." *Science* 318: 245–250.

Minh, B. Q., H. A. Schmidt, O. Chernomor, et al. 2020. "IQ-TREE 2: New Models and Efficient Methods for Phylogenetic Inference in the Genomic Era." *Molecular Biology and Evolution* 37: 1530–1534.

Murik, O., L. Tirichine, J. Prihoda, et al. 2019. "Downregulation of Mitochondrial Alternative Oxidase Affects Chloroplast Function, Redox Status and Stress Response in a Marine Diatom." *New Phytologist* 221, no. 3: 1303–1316. https://doi.org/10.1111/nph.15479.

Obata, T., S. Schoenefeld, I. Krahnert, S. Bergmann, A. Scheffel, and A. Fernie. 2013. "Gas-Chromatography Mass-Spectrometry (GC-MS) Based Metabolite Profiling Reveals Mannitol as a Major Storage Carbohydrate in the Coccolithophorid Alga *Emiliania huxleyi*." *Metabolites* 3, no. 1: 168–184.

Palmieri, F. 2013. "The Mitochondrial Transporter Family SLC25: Identification, Properties and Physiopathology." *Molecular Aspects of Medicine* 34, no. 2–3: 465–484. https://doi.org/10.1016/j.mam.2012.05.005.

Palmieri, F., and C. L. Pierri. 2010. "Structure and Function of Mitochondrial Carriers – Role of the Transmembrane Helix P and G Residues in the Gating and Transport Mechanism." *FEBS Letters* 584, no. 9: 1931–1939. https://doi.org/10.1016/j.febslet.2009.10.063.

Palmieri, F., C. L. Pierri, A. De Grassi, A. Nunes-Nesi, and A. R. Fernie. 2011. "Evolution, Structure and Function of Mitochondrial Carriers: A Review With New Insights." *Plant Journal* 66, no. 1: 161–181. https://doi.org/10.1111/j.1365-313X.2011.04516.x.

Petersen, J., K. Förster, P. Turina, and P. Gräber. 2012. "Comparison of the H+/ATP Ratios of the H+-ATP Synthases From Yeast and From Chloroplast." *Proceedings of the National Academy of Sciences of the United States of America* 109, no. 28: 11150–11155. https://doi.org/10.1073/pnas.1202799109.

Petersen, J., A. K. Ludewig, V. Michael, et al. 2014. "Chromera Velia, Endosymbioses and the Rhodoplex Hypothesis—Plastid Evolution in Cryptophytes, Alveolates, Stramenopiles, and Haptophytes (CASH Lineages)." *Genome Biology and Evolution* 6: 666–684.

Petersen, T. N., S. Brunak, G. von Heijne, and H. Nielsen. 2011. "SignalP 4.0: Discriminating Signal Peptides From Transmembrane Regions." *Nature Methods* 8, no. 10: 785–786. https://doi.org/10.1038/nmeth.1701.

Picault, N., L. Palmieri, I. Pisano, M. Hodges, and F. Palmieri. 2002. "Identification of a Novel Transporter for Dicarboxylates and Tricarboxylates in Plant Mitochondria. Bacterial Expression, Reconstitution, Functional Characterization, and Tissue Distribution." *Journal of Biological Chemistry* 277, no. 27: 24204–24211. https://doi.org/10.1074/jbc.M202702200.

Prihoda, J., A. Tanaka, W. B. M. de Paula, J. F. Allen, L. Tirichine, and C. Bowler. 2012. "Chloroplast-Mitochondria Cross-Talk in Diatoms." *Journal of Experimental Botany* 63, no. 4: 1543–1557.

Rastogi, A., O. Murik, C. Bowler, and L. Tirichine. 2016. "PhytoCRISP-Ex: A Web-Based and Stand-Alone Application to Find Specific Target Sequences for CRISPR/CAS Editing." *BMC Bioinformatics* 17, no. 1: 261.

Riazunnisa, K., L. Padmavathi, H. Bauwe, and A. S. Raghavendra. 2006. "Markedly Low Requirement of Added CO_2 for Photosynthesis by Mesophyll Protoplasts of Pea (*Pisum sativum*): Possible Roles of Photorespiratory CO_2 and Carbonic Anhydrase." *Physiologia Plantarum* 128, no. 4: 763–772.

Ruprecht, J. J., and E. R. S. Kunji. 2020. "The SLC25 Mitochondrial Carrier Family: Structure and Mechanism." *Trends in Biochemical Sciences* 45, no. 3: 244–258. https://doi.org/10.1016/j.tibs.2019.11.001.

Satre, M., S. Mattei, L. Aubry, et al. 2007. "Mitochondrial Carrier Family: Repertoire and Peculiarities of the Cellular Slime Mould *Dictyostelium discoideum*." *Biochimie* 89, no. 9: 1058–1069. https://doi.org/10.1016/j.biochi.2007.03.004.

Seydoux, C., M. Storti, V. Giovagnetti, et al. 2022. "Impaired Photoprotection in *Phaeodactylum tricornutum* KEA3 Mutants Reveals the Proton Regulatory Circuit of Diatoms Light Acclimation." *New Phytologist* 234, no. 2: 578–591. https://doi.org/10.1111/nph.18003.

Shikanai, T. 2007. "Cyclic Electron Transport Around Photosystem I: Genetic Approaches." *Annual Review of Plant Biology* 58: 199–217. https://doi.org/10.1146/annurev.arplant.58.091406.110525.

Simion, P., H. Philippe, D. Baurain, et al. 2017. "A Large and Consistent Phylogenomic Dataset Supports Sponges as the Sister Group to All Other Animals." *Current Biology* 27: 958–967.

Smith, S. R., C. L. Dupont, J. K. McCarthy, et al. 2019. "Evolution and Regulation of Nitrogen Flux Through Compartmentalized Metabolic Networks in a Marine Diatom." *Nature Communications* 10: 4552. https://doi.org/10.1038/s41467-019-12407-y.

Uwizeye, C., J. Decelle, P.-H. Jouneau, et al. 2021. "Morphological Bases of Phytoplankton Energy Management and Physiological Responses Unveiled by 3D Subcellular Imaging." *Nature Communications* 12, no. 1: 1049. https://doi.org/10.1038/s41467-021-21314-0.

van Kempen, M., S. S. Kim, C. Tumescheit, et al. 2024. "Fast and Accurate Protein Structure Search With Foldseek." *Nature Biotechnology* 42, no. 2: 243–246. https://doi.org/10.1038/s41587-023-01773-0.

Van Vlierberghe, M., A. Di Franco, H. Philippe, and D. Baurain. 2021. "Decontamination, Pooling and Dereplication of the 678 Samples of the Marine Microbial Eukaryote Transcriptome Sequencing Project." *BMC Research Notes* 14: 306.

Van Vlierberghe, M., H. Philippe, and D. Baurain. 2021. "Broadly Sampled Orthologous Groups of Eukaryotic Proteins for the Phylogenetic Study of Plastid-Bearing Lineages." *BMC Research Notes* 14, no. 1: 143.

Varadi, M., D. Bertoni, P. Magana, et al. 2024. "AlphaFold Protein Structure Database in 2024: Providing Structure Coverage for Over 214 Million Protein Sequences." *Nucleic Acids Research* 52, no. D1: D368–D375.

Villanova, V., A. E. Fortunato, D. Singh, et al. 2017. "Investigating Mixotrophic Metabolism in the Model Diatom *Phaeodactylum tricornutum*." *Philosophical Transactions of the Royal Society, B: Biological Sciences* 372, no. 1728: 20160404.

Villanova, V., D. Singh, J. Pagliardini, et al. 2021. "Boosting Biomass Quantity and Quality by Improved Mixotrophic Culture of the Diatom *Phaeodactylum tricornutum*." *Frontiers in Plant Science* 12: 642199. https://doi.org/10.3389/fpls.2021.642199.

Supporting Information

Additional supporting information can be found online in the Supporting Information section. **Data S1:** ppl70640-sup-0001-Supinfo.pdf.